

Structure-function relationship for functional films with constructed graded channels in dye/salt separation and fouling resistance

Desalination

Zhang, Tianmeng; Zhang, Weiwei; Yang, Xiaoyan; Zuilhof, Han; Lu, Hao https://doi.org/10.1016/j.desal.2024.118262

This publication is made publicly available in the institutional repository of Wageningen University and Research, under the terms of article 25fa of the Dutch Copyright Act, also known as the Amendment Taverne.

Article 25fa states that the author of a short scientific work funded either wholly or partially by Dutch public funds is entitled to make that work publicly available for no consideration following a reasonable period of time after the work was first published, provided that clear reference is made to the source of the first publication of the work.

This publication is distributed using the principles as determined in the Association of Universities in the Netherlands (VSNU) 'Article 25fa implementation' project. According to these principles research outputs of researchers employed by Dutch Universities that comply with the legal requirements of Article 25fa of the Dutch Copyright Act are distributed online and free of cost or other barriers in institutional repositories. Research outputs are distributed six months after their first online publication in the original published version and with proper attribution to the source of the original publication.

You are permitted to download and use the publication for personal purposes. All rights remain with the author(s) and / or copyright owner(s) of this work. Any use of the publication or parts of it other than authorised under article 25fa of the Dutch Copyright act is prohibited. Wageningen University & Research and the author(s) of this publication shall not be held responsible or liable for any damages resulting from your (re)use of this publication.

For questions regarding the public availability of this publication please contact openaccess.library@wur.nl

ELSEVIER

Contents lists available at ScienceDirect

Desalination

journal homepage: www.elsevier.com/locate/desal



Structure-function relationship for functional films with constructed graded channels in dye/salt separation and fouling resistance

Tianmeng Zhang ^a, Weiwei Zhang ^b, Xiaoyan Yang ^c, Han Zuilhof ^{d,e}, Hao Lu ^{a,*}

- a Department of Materials and Textile Engineering, G60 STI Valley Industry & Innovation Institute, Jiaxing University, Jiaxing, Zhejiang 314001, PR China
- b Department of Architecture and Civil Engineering, City University of Hong Kong, Kowloon, Hong Kong, China
- c Institute of Advanced Ceramic Material and Fiber, School of Materials Science and Engineering, Zhejiang Sci-Tech University, Hangzhou 310018, PR China
- ^d China-Australia Institute for Advanced Materials and Manufacturing, Jiaxing University, Jiaxing 314001, PR China
- ^e Laboratory of Organic Chemistry, Wageningen University, 6708 WE Wageningen, the Netherlands

ARTICLE INFO

Keywords: Separation film Film surface structure Separation behavior Dye/salt separation

ABSTRACT

The structural assembly of polypyrrole particle stacking, combined with polydopamine space-filling, forms composite film with a network of interconnected fluid channels. The composite films achieve high water flus, separation efficiency and ratio of organic dyes/inorganic salts (flux: $>600 \, L \, m^{-2} \, h^{-1} \, bar^{-1}$; dye rejection: $\sim 100 \, W$; salt rejection: $<5 \, W$). Simulation using different dye fouling models show that the dye only interacts at the surface, and hardly affects internal pores of the film throughout the filtration process. Owing to the patterned surface structure as constructed by microsphere arrangement and inter-structure adaptation assembly, the functional film has excellent contamination tolerance and rinsing regeneration for macromolecular pollutants. The results of computational fluid dynamics simulations further indicate that the high shear stress above the microspheres with vortex flow in the interstitial space has a positive effect on reducing contaminant deposition. In addition to the separation property, the composite film shows good structural stability and mechanical strength in various complex water environments, benefiting their future practical applications. This work unveils the structure-function relationship for composite function films with constructed graded channels in dye/salt separation, which is important for the design and future application of these functional films.

1. Introduction

Efficient deep wastewater treatment is of essential importance for environmental protection. Undesired interactions and mixing between organic solutes and salts greatly limit the efficiency during wastewater treatment. The challenge is further manifested from the perspectives of the harmless degradation of (bio-)organic matter and the resource recovery of salt ions [1]. The efficient separation of organic materials from inorganic salts is generally a crucial step in the treatment of organic/salt wastewater [2]. Separation technology [3] using porous films shows advantages in terms of its high flow, high efficiency, ease of operation, and significant energy savings, therefore, porous films are important membrane materials for separating organic materials and inorganic salts.

In order to improve the separation performance of the porous film, several designing strategies have been used. For instance, non-planar structural units were introduced into rigid polymers [4,5], by

controlling the phase transition processes [6,7], in this way both the structure and chemistry of the film can be regulated in a synergistic manner. In addition, ultra-thin films with high mechanical strength were developed to enhance the water transport and ion separation [8,9]. Despite great efforts, the problems of long transmission paths and high mass transfer resistance – mainly owing to poor inter-pore penetration – have still not been effectively solved. Constructing continuously graded pores combining high-flux macropores and high-rejection micropores, is a promising approach for the efficient separation of organics/salt [10,11]. For instance, ZIF-8@GO films [12] with nano- and subnanostructures have achieved a significant improvement in separation selectivity, water flux, and film stability. Furthermore, porous films with interconnected pores covering the entire range from micro- via meso- to macropores showed great improvement in the diffusion and separation efficiency for oil-water emulsions [13].

Despite that the designing strategies of such graded pore structures have been extensively researched [14,15], there are at least still two

E-mail address: lu@zjxu.edu.cn (H. Lu).

^{*} Corresponding author.

fundamental questions not answered yet: (1) for separating the target solutes by functional film, what is the distribution of solutes and their interaction mechanism at the film surface? (2) for a stable and prolonged use of functional film in even harsh conditions [16,17], what is the structure designing principle for designing the functional film?" In particular, the functional film often faces erosion and pore blocking by pollutants, which breaks the graded pore structure and strongly reduces the service lifetime of the film. So far, it remains a challenge to rationally grasp the orchestrated balance between the structural adaptation of graded pore channels, and the long-term separation behavior of the target solutes.

The particle stacking model was derived from natural sand and gravel structures for water purification [18], the structural design principles for thin-film separations based on such particle stacking models have enabled quantitative optimization of microstructural parameters such as film thickness/porosity/porosity [19]. In addition, patterned surface structures formed by particle arrangements have further reduced membrane contamination by enhancing mass transfer and water flow [20].

In this work, based on a particle stacking model, structurally stable and contamination-resistant composite films with graded-channel materials were successfully fabricated (see Fig. 1, for a schematic representation). The design parameters of the composite films were systematically optimized using the model, and the resulting films were applied for the selective separation for dyes/salts. Importantly, the detailed features of the interactions relevant for organic/salt separation and fouling resistance have been elucidated from multiple perspectives: First, using four fouling models, the distribution of dye molecules on pore surface has been clarified. Second, the separation of complex fouling mixtures was further explored for the composite films, and the resistance mechanism based on graded-channels was unveiled by hydrodynamic simulations. Finally, the effects of the structurally composite nature of these films on the stability and mechanical properties have been clarified, outlining their applications in versatile complex

aqueous environments.

2. Results and discussion

2.1. Fabrication of PPMs film and performance for water permeance

Drawing inspiration from the natural purification process of groundwater by sand and gravel soil (Fig. S1), film materials with a graded fluid pore channel were constructed through particle stacking and space-filling, in order to efficiently separate organic matter/inorganic salts. Fig. 2 illustrates the fabrication and microstructure of the functional PPMs (polydopamine-coated polypyrrole microspheres) film. Details on the preparation of the membrane can be found in "Experimental procedures" in the SI. Both polydopamine and polypyrrole are common polymer materials, which, according to previous literatures [21-24], have been well applied for preparation and modification of membrane materials. Non-cross-linked cellulose coated with polypyrrole served as substrate, and polydopamine-functionalized polypyrrole microspheres, having the thickness of ~ 9 µm as illustrated in Fig. S2, were used as the functional layer. The macropores formed by the stacking of polypyrrole microspheres and the cross-linked micropores formed by polydopamine filling are coupled in series with each other, and interconnected permeation channels were achieved from the assembled structure. Our recent study has demonstrated the feasibility of this preparation strategy for achieving high-performance composite films [25]. The cross-section micrographs of the PPMs film (Fig. S3) reveal that the thickness of the PBC (polypyrrole-coated bacterial cellulose) basal layer is much larger than that of the microsphere layer. Elemental mapping results show a homogeneous distribution of the elements C, O, N (Fig. S2). The assembled fibrous PBC structure renders the functional PPMs film good flexibility and self-supporting properties, that can be easily peeled off from the substrate surface.

To obtain the optimal film material for detailed property and application study. Parameter optimization was carried out using

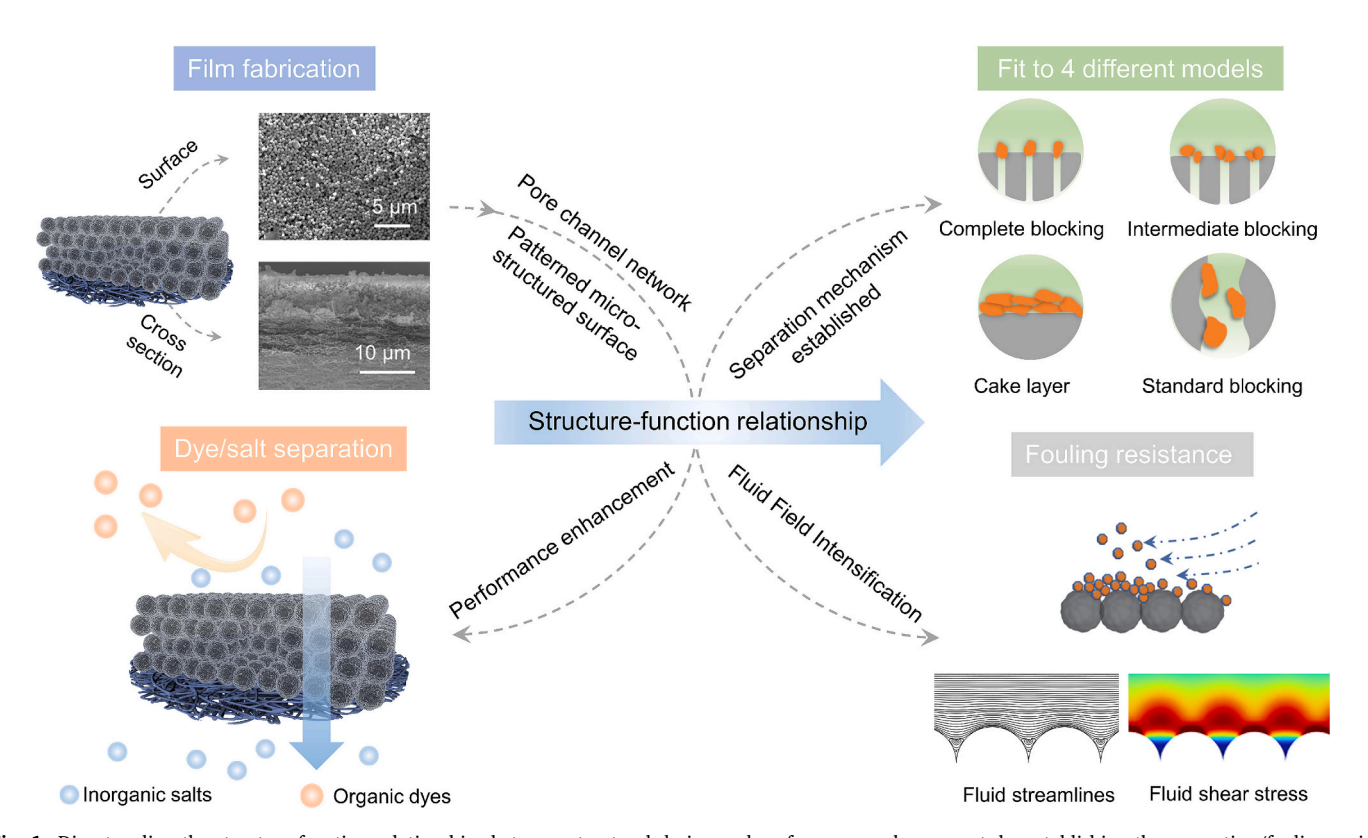


Fig. 1. Disentangling the structure-function relationships between structural design and performance enhancement, by establishing the separation/fouling resistance mechanisms.

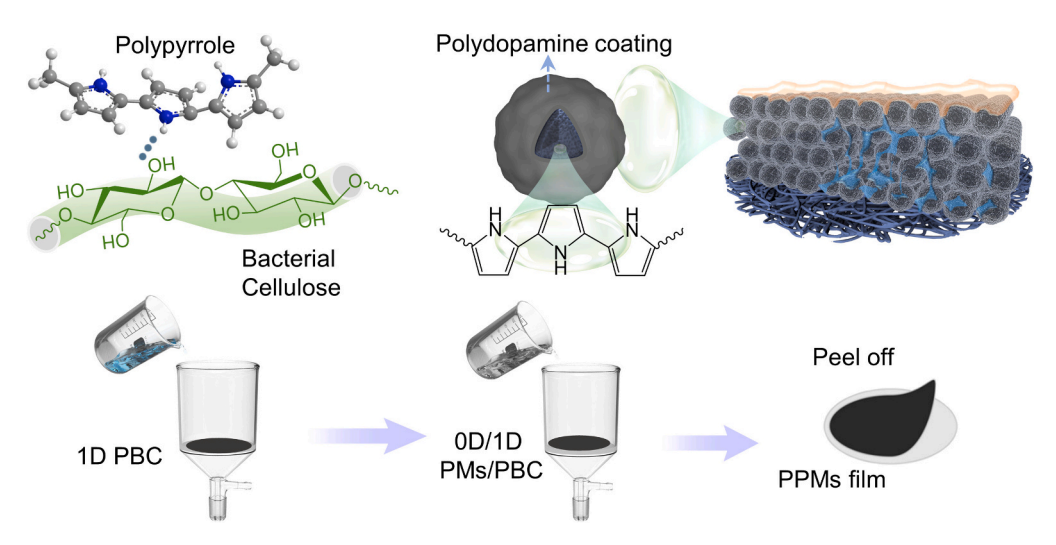


Fig. 2. Schematic diagram illustrating the fabrication and microstructure of PPMs film.

experimental design at the Box-Behnken level of response surface methodology. The overall water flux was calculated by optimization of the three experimental parameters, namely thickness of PBC layer (X1, μm), thickness of microsphere layer (X2, μm) and inlet pressure (X3, bar) on the pure water flux (calculation details and underlying data in Tables S1 and S2). Fig. 3 shows the three-dimensional surface and contour plots, which were used to disentangle the crossing effects of those three parameters above. With increasing the thickness of PBC layer over the range from 38 to 110 µm, the film permeability starts to decrease significantly, and finally reaches a nearly constant value (Fig. 3a, b). The increasing thickness of the PBC layer has a greater effect on reducing the pure water flux, which is probably due to the entanglement of PBC fibers within the film (fiber structure in Fig. S3). The mass transfer resistance of water increases exponentially with the increasing thickness, which is consistent with the law of the "back-offoot" model of previous studies [26]. Compared to the thickness of the PBC layer, the thickness of the microsphere layer has a much smaller effect on water flux (Fig. 3c, d). Despite the increase of its thickness, the special nanofluidic pore networks constructed by microspheres, along with the hydrophilic functional groups, enhance water mass transfer in aqueous flow. In addition, the increase in inlet pressure showed an

approximately linear enhancement of water flux (Fig. 3e, f). Through the ANOVA (Analysis of Variance) of the regression model under the BBD level of the response surface method (Table S3), the relative influence of different parameters on the water flux can be summarized as follows: thickness of PBC layer > inlet pressure > thickness of microsphere layer. Several factors were also considered for practical applications, such as the self-supporting nature of the films, dye rejection, and the cost. The loading of PBCs was limited to 26.7–33.3 g•m $^{-2}$, and load of microspheres was 5–12 g•m $^{-2}$.

2.2. Dye/salt separation for PPMs films

PPMs film obtained by the optimized preparation process were systematically tested for its separation performance. The separation of organic dyes was tested by dead-end filtration (Fig. S4). The separation efficiency depends on the molecular weight of the dyes (Fig. 4a): the rejection rate is ~ 100 % for the dyes with molecular weight > 400 Da, irrespective of the charge of the dyes; for the dyes with molecular weight between 300 and 400 Da, the rejection rate is still higher than 85 %, but varies in terms of different dyes. In addition, some small organic molecules such as urea, piperazine, lactic acid, melamine, glucose, and

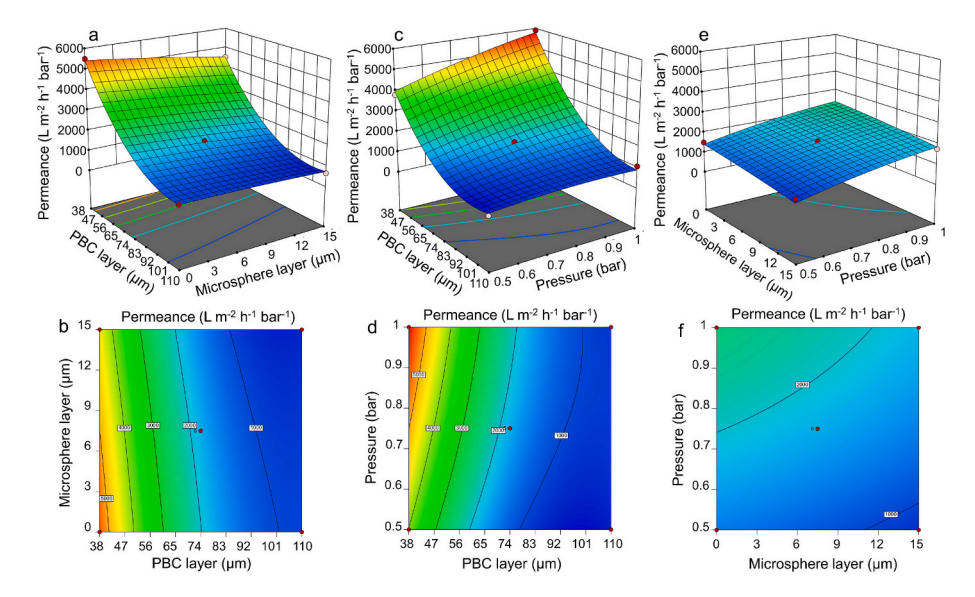


Fig. 3. Three-dimensional surfaces (a, c, e) and contour plots (b, d, f) disentangling the mutual interdependence for three parameters, including: thickness of the one-dimensional PBC layer, thickness of microsphere layer, and pressure on film permeance flux.

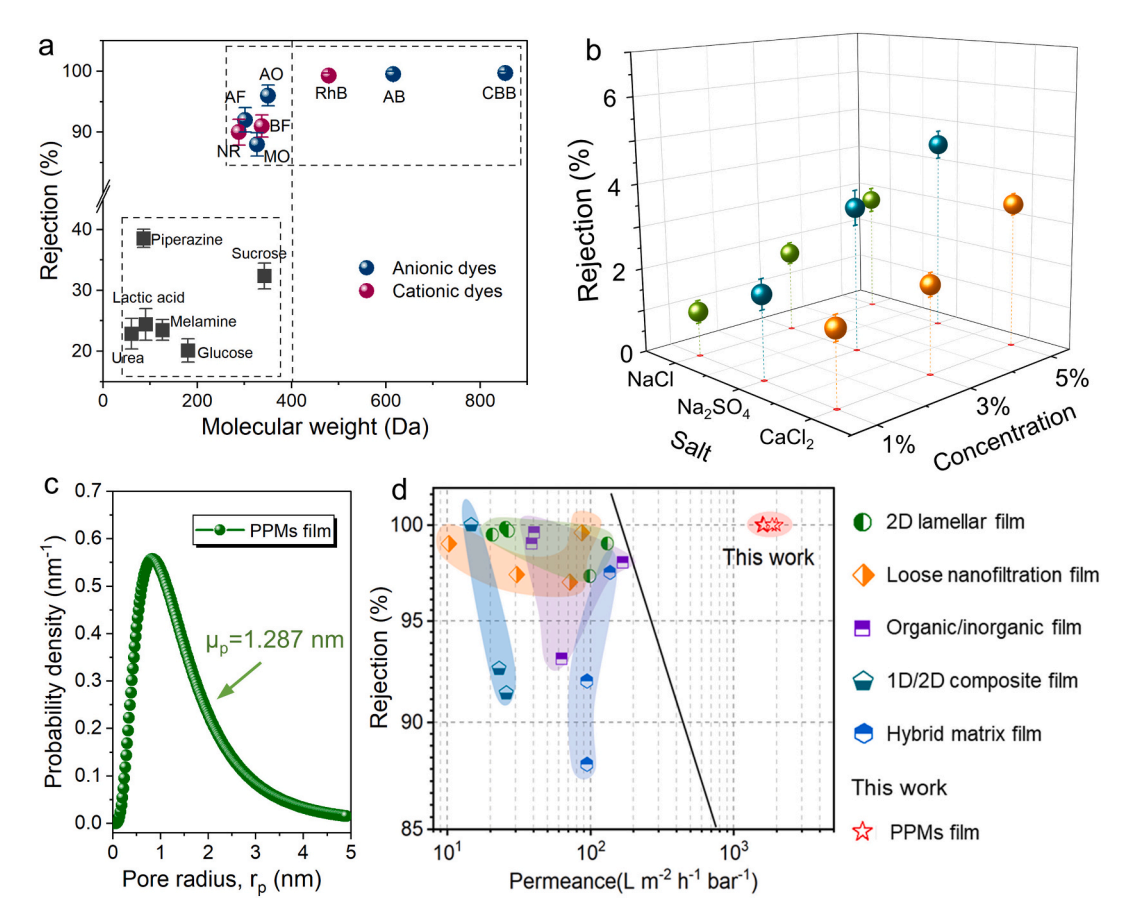


Fig. 4. Separation performance of PPMs film: (a) Rejection rates for various organic dyes with different molecular weight (NR: Neutral red; AF: Acid fuchsin; MO: Methyl orange; BF: Basic fuchsin; AO: Acid orange; RhB: Rhodamine B; AB: Acid black; CBB: Coomassie brilliant blue); (b) Rejection rates for different inorganic salts with different concentration; (c) Pore size distribution as derived from rejection rates for PEGs, see text for details. (d) Comparison of dye separation performance of composite films in this study and other studies. (For interpretation of the references to color in this figure legend, the reader is referred to the web version of this article.)

sucrose were also tested for separation performance of PPMs films. The rejection rates were generally lower than 40 %, and also varies with organic molecules of different size and structure. In stark contrast to the high rejection of organic dyes, PPMs film have a high permeability to different inorganic salts (Fig. 4b), indicating the selective dye/salt separation. The rejection rates for PEG with varying molecular weight were tested (Fig. S5). Based on the relationship between MWCO (molecular weight cutoff) and Stokes radius, a lognormal model of the pore radius distribution was created with a cutoff curve and a probability density function between cutoff and Stokes radius [27]. The average pore size of the PPMs film was ~1.29 nm (Fig. 4c), this value is higher than the diameter of salt ions, while lower than the diameter of dyes. In particular, taking into account of the aggregation nature of dyes (Fig. S6), the \sim 1.29 nm nanopores of PPMs are adequately suitable for separating the dye/salt. The normal distribution of pore sizes showed that the PPMs films had a wide distribution for pore size, which was related to the gradient pore structure, i.e., the macropores are stacked by the polypyrrole spheres, and the micropores are filled by the polydopamine interstitials (Fig. 2, upper right). Furthermore, the highly negative charge of PPMs (Fig. S7) explains the higher rejection rate for anionic dyes as compared to cationic ones. The excellent dye/salt separation performance for PPMs film is also reflected in comparison with the data reported in the previous literatures: the water flux is 1-2 orders of magnitude higher than those reported values, while rejection rate of dyes is nearly 100 % (Figs. 4d, S8 and Table S4).

The self-made cross-flow device is also used to test the selective separation of dyes/salts for the composite film (Fig. S9). We examined the laws affecting water flux and selective rejection as a function of concentration, for dye (Fig. S10) and salt (Fig. S11). On the one hand, the increase in dye concentration increases the chance of contact between the dyes and PPMs film, which results in the accumulation of the dyes and thereby reduces water permeation (Fig. S10). On the other hand, increasing salt concentration leads to larger clusters of the dyes, which causes lower water flux and higher salt rejection rate (Fig. S11). These additional analysis from cross-flow device, again, point to the fact that the PPMs film is ideal for selective separation for dyes/salts.

2.3. Separation mechanism for PPMs films

To better understand the separation mechanism for PPMs films, we used a mathematical theoretical model to explore the presence and distribution of dyes on the film surface during separation. The separation process is influenced by multilevel factors between the film surface and the targeted solute (Fig. S12). Darcy's law [28] (Eq. S-14) was used to calculate interfacial forces in film mass transfer, and to determine the maximum effect of fouling resistance on film fluxes (Fig. S13). The presence state of the target solute on the film surface has been categorized into four typical models (Fig. S14), which represent the different distributions of the solute in the nanopores. Modified mathematical models (Eq. S-15/S-16) were applied to fit kinetic data of water flux during separation.

We analyzed the separation process for a typical RhB solution (10 mg $\rm L^{-1}$; measurements at room temperature), Fig. 5 presents the variation in terms of the normalized water flux. In the initial stage, the enrichment of RhB dyes on the film surface leads to a rapid decrease in permeate flux (Fig. 5a). As the surface density of RhB at the surface

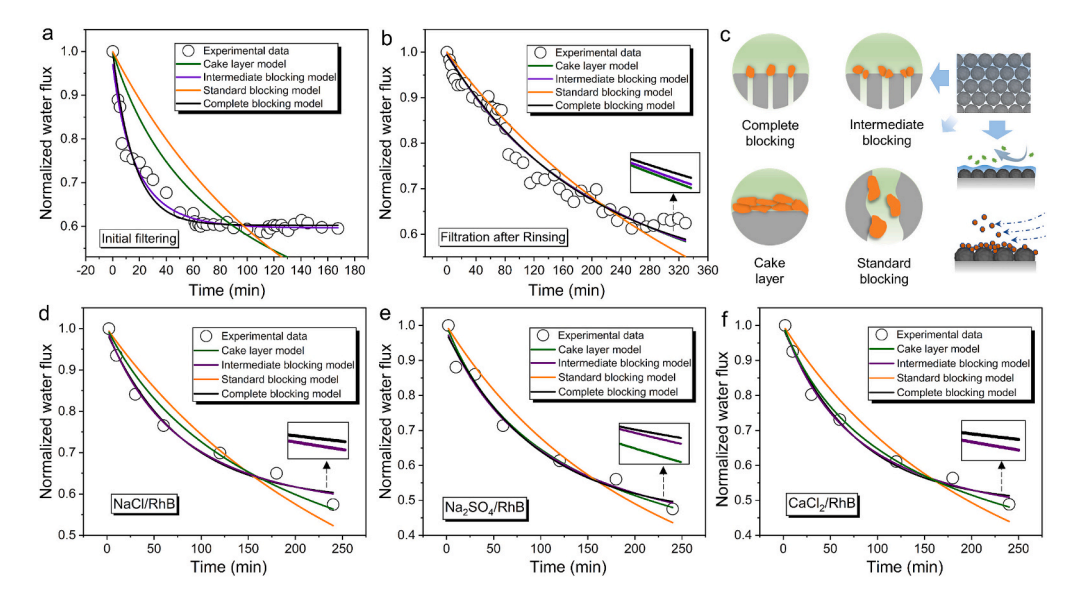


Fig. 5. Separation behavior of dyes at the surface of PPMs film: **(a)** Filtration separation data and the fitting using different models; **(b)** Filtration separation data and fitting for PPMs film after rising; **(c)** Dye fouling models on the surface of PPMs film; **(d-f)** Filtration separation data and fitting plot of PPMs films, for **(d)** NaCl/RhB, **(e)** Na₂SO₄/RhB, **(f)** CaCl₂/RhB separations.

increases, the accumulation of dye leads to a dynamic equilibrium with the diffusion into water. Thus, the osmotic flux of the dye solution was essentially stable after 60 min of filtration. The experimental data were fitted using the cake layer model, the intermediate blocking model, the standard blocking model, and the complete blocking model for the 180min filtration process. Table 1 summarizes the degree of agreement between the experimental data and the fitted function. The fitted correlation coefficients of the cake layer model and the standard blocking model are $R^2 = 0.411$ and $R^2 = -0.060$, respectively, which indicate that the regression curves are poorly fitted to the experimental values and cannot explain the separation behavior of the dyes on the PPMs films. In contrast, the intermediate blocking model ($R^2 = 0.969$) and the complete blocking model (R² = 0.963) yield significantly better fits, which is also apparent from the curves in Fig. 5a. The dye separation behavior for PPMs film after pure water rinsing was also analyzed. As seen in Fig. 5b, the water fluxes decay in a much slower trend, comparing to that before rinsing. The rinsing step changes the surface property of PPMs film, which in turn affects their separation behavior. Table 1 reveals all four models have similar, good fitting results, and the fitting coefficients R² are 0.959, 0.964, 0.917, 0.967, respectively, which suggests that changing film surface property affects dye filtration. The difference in water flux trends before and after flushing is possibly due to the residual irreversible contamination on the pore structure, which change the film surface properties and thus affects the interaction force with the dyes. However, it is still obvious that the intermediate blocking

Table 1The degree of agreement between the experimental data and the fitted function based on the underlying model for initial filtration, filtration after rinsing with pure water, and for filtration of composite salt/dye solutions.

Filtration process; salt/ dye	Model fit (R ²)			
	Cake layer model	Intermediate blocking model	Standard blocking model	Complete blocking model
Initial filtration	0.411	0.969	-0.060	0.963
Filtration after rinsing	0.959	0.964	0.917	0.967
NaCl/RhB	0.980	0.984	0.819	0.978
Na ₂ SO ₄ /RhB	0.976	0.978	0.931	0.975
CaCl ₂ /RhB	0.987	0.992	0.928	0.987

model and the complete blocking model (Fig. 5c) work better than the other two models. Our additional results (Fig. S15) imply that the adsorption effect by functional PPMs layer can be ignored as compared to the fiber layer PBC.

Next, the separation of mixed NaCl/RhB, Na₂SO₄/RhB, and CaCl₂/RhB solutions (salt concentrations 1 wt%; dye concentrations: 5 mg L⁻¹) were further analyzed by fitting the four aforementioned contamination models. Fig. 5(d-f) compare the four models when predicting the measurements. As seen from different color curves, the data by the intermediate blocking model and the complete blocking model fit better to the measured values. The better fits of these two models are in agreement with the data for the single-component dye separation, implying separation of the dyes on the film surface is not so much affected by the presence of salt ions. The fitted correlation coefficients R² in Table 1 reinforce these conclusions.

Based on the theoretical modeling in Fig. 5, it was concluded that during the separation of dyes/salts by PPMs films, the dyes are mainly enriched on the film surface in the form of contaminants, which change the film surface properties and pore surface structure, and thus affect the permeate flux. The enrichment process only occurs in the initial filtration period, while reaches saturation with the extension of time. From the characteristics of the intermediate blocking model and the complete blocking model, the dyes mainly adsorb the surface pores of the PPMs films, completely or partially clogs the pores. Protection of internal pore network [29] is positive for the durable high flux and long-term stability of the functional PPMs film.

2.4. Fouling resistance and mechanism of PPMs film

Grasping the dye/salt separation mechanism of PPMs films prompted us to extend their application to organic fouling resistant materials. This is of particular practical relevance, since these fouling deposits often influence the separation process in a negative way, yielding a reduced water quality, shortened film lifetime, reduced flux, and – as a result of all these - also increased operating costs [30,31]. We thus studied the contamination resistance of PPMs film, and analyzed the effect of surface microstructure for contamination resistance. To this aim we show in Fig. 6a-b the variation in terms of normalized water flux for PBC and PPMs composite films, after contamination with bovine serum albumin (BSA) and humic acid (HA), respectively. The contamination of the film surface continued to increase with the filtration time of both the BSA and

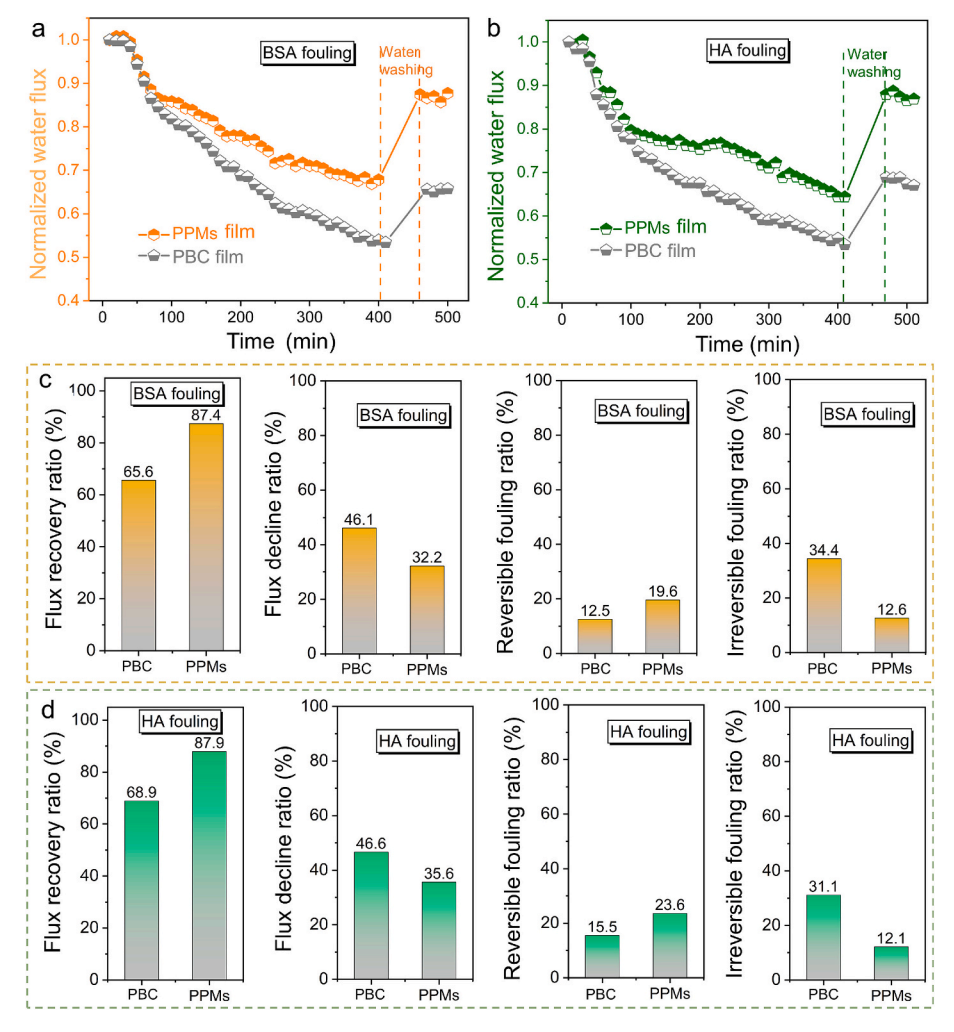


Fig. 6. Fouling resistance for PMs and PPMs composite films: (a, b) Normalized flux changes of PPMs and PMs films, for fouling resistance of BSA (a) and HA (b); (c-d) Comparing fouling resistance between PMs and PPMs films for BSA (c) and HA (d), in terms of: Flux recovery ratio; Flux decay value; Reversible fouling ratio; Irreversible fouling ratio.

HA solutions, resulting in a gradual decrease in the flux of PBC and PPMs films. When the filtration time reached 400 min, the post-contamination normalized water fluxes were 0.53 (BSA) and 0.52 (HA) for PBC films, while the corresponding post-contamination normalized water fluxes for PPMs films were 0.67 (BSA) and 0.64 (HA). Apparently, the normalized water flux of PPMs films was always higher than that of PBC films, indicating that the surface of PPMs films is slightly more resistant to fouling. After rinsing with pure water, the water fluxes for both films increased again to normalized fluxes of 0.87 and 0.88 respectively, indicating that physically adsorbed BSA and HA adhering to the film surface could be washed away by the water flow.

The data during the contamination process was further analyzed. The flux recovery ratio (FRR), flux decay value (FDR), reversible fouling ratio (FRr) and irreversible fouling ratio (FRir) of the composite films were calculated to analyze the performance of the composite films in terms of resistance to BSA and HA fouling. Fig. 6c and d compare these contamination-related variables for PMs and PPMs films, after contamination of BSA and HA, respectively. For both two cases, the higher the flux recovery ratio and reversible fouling ratio, together with the lower the corresponding flux attenuation value and irreversible fouling ratio, all suggest the higher fouling resistance for PPMs film. For PPMs functional films, the special microsphere arrangement structure creates roughness and modify the hydrophilicity of the film surface, which has additional repulsive effect on fouling contaminants. It is thus particularly noteworthy that on our PPMs films, the recovery was significantly

higher than on the corresponding PBC films, indicating the potential of our materials, which promises significantly enhanced device lifetimes when filters are used in combination with back-pulsing schemes or mixing in of specific anti-fouling materials like zwitterionic polymers [32,33].

Fig. 7 shows the microscopic morphology of the PPMs films and the reference PBC films before (a, d) and after (b, e, g) contaminant solution for 400 min, as well as after water washing afterwards (c, f, h). PBC films show fibrous features, while the PPMs films show uniform structure of microspheres. After cross-flow filtration, the PBC film surface accumulates a large amount of contaminant deposition (raised folds formed by contaminant aggregation in (b)); whereas the same contaminant deposition layer is much thinner on PPMs films (visible surface microsphere morphology in (e, g)). After further water washing, the contaminants on the surface of PBC retained, and the original fiber structure still could not be discerned; by comparison, the PPMs film showed an obvious contaminant shedding feature (presenting pore-like erosion area in (f, h)) after water washing, and the morphological structure of the microspheres became clearer. Table S5 shows the percentage of elemental content on the face-swept surface of the film, and the change in elemental composition before and after contamination indicates the presence of fouling BSA (HA) on the film surface.

Overall, the data in Figs. 6 and 7 provide clear evidence that PPMs films have much an improved anti-fouling performance compared to PBC films without surface modification. We hypothesized that this was

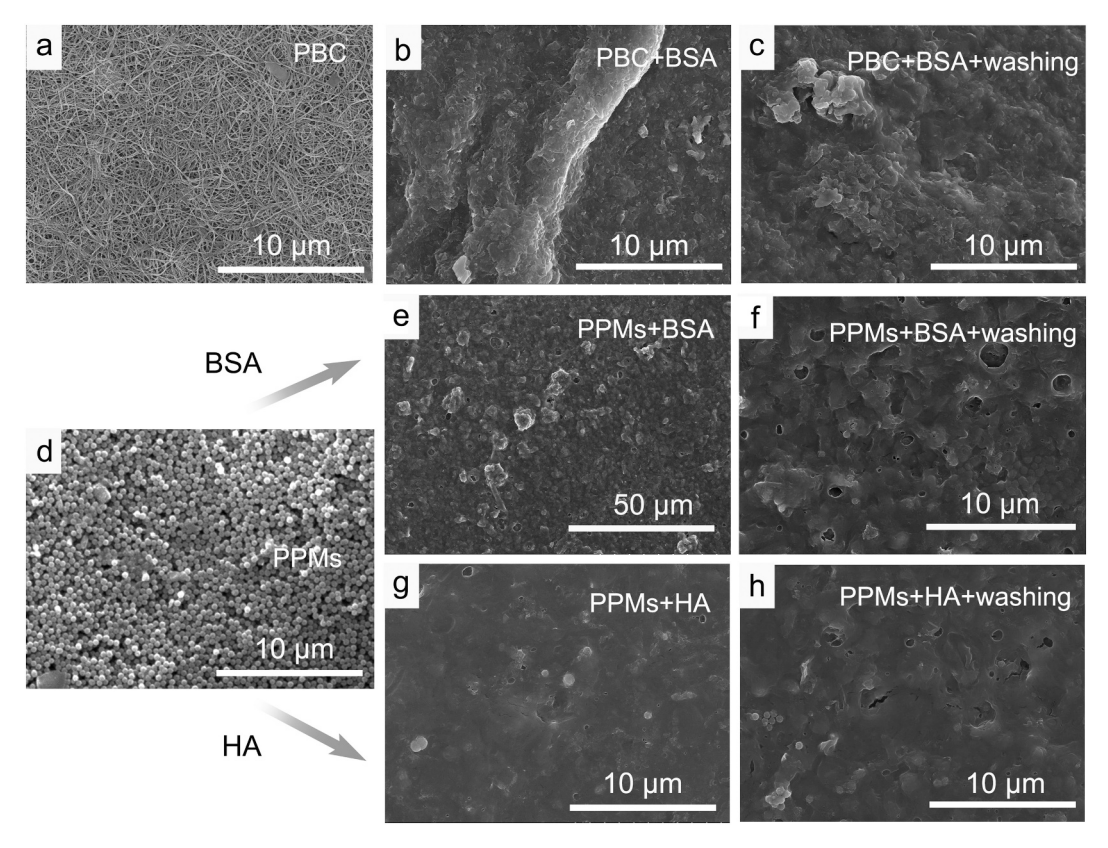


Fig. 7. SEM images of the composite film before and after 400 min of BSA and HA fouling, and after 20 min of water washing afterwards. Before fouling: (a) PBC film, (d) PPMs film; After fouling: (b) PBC film (BSA fouling), (e) PPMs film (BSA fouling), (g) PPMs film (HA fouling); after washing: (c) PBC film (BSA fouling), (f) PPMs film (BSA fouling), (h) PPMs film (HA fouling).

caused by the fact that these PPMs films are enriched with a microsphere-constructed fluid pore structure. In this geometry, the water flow should be accelerated, leading to the more efficient removal of fouling materials at the surface [34]. To better validate this idea, we explored the process through fluid dynamics simulations. The CFD (Computational Fluid Dynamics) analysis was used to study the fluid flow characteristics of spherical patterned shapes in comparison to flat film structures. The optimized number of elements was determined to be 6556 for the flat geometry, and 18,590 for spherical pattern geometry (Fig. 8a-b). The state of the fluid streamline distribution in the x-coordinate region from 2 µm to 3.5 µm is shown in Fig. 8c-d. The flow lines in the flat film show relatively uniform parallel streamlines, and the fluid flow remains relatively homogeneous. In contrast, vortices are observed in the valley region between the spherical patterns. The drastic inhomogeneity in the local flow characteristics is caused by the patterned geometry, and the vortex flow characteristics strongly reduce fouling. According to previous literature [35], larger aggregates are predominantly forming at the valley region. In this context, the shear stress generated by fluid flow plays an active role for the removal of the contaminants from the surface. Fig. 8e-f quantitatively show the fluid shear stress distribution on the surface of two different structural films. The shear stresses were uniformly distributed over the flat film, and a trend from high to low stresses from the wall to the center was observed. Again, in stark contrast, the shear stresses around the spherical pattern were unevenly distributed, generating higher shear stresses near the top of the spherical pattern and lower shear stresses in the center and valley regions. Therefore, the microsphere stacking effectively generates much localized turbulence in the vicinity of the pattern [20]. These gradient shear stresses regions are connected continuously, and mutually enhance the hydrodynamic conditions on the film surface, thus leading to much improved fouling resistance under flow conditions.

2.5. Stability and mechanical properties of PPMs film

The application of composite films under flow conditions necessitates the stability and strength of the PPMs films. The stability of such composite film materials in aqueous environments is on a molecular scale affected by a number of aspects, including the polar attraction with water molecules, ions, and molecules, as well as the solution pH [36]. In principle, the regular spheres of polypyrrole microspheres are isolated, and therefore easily detached from the PMs film by the polar water molecules, resulting in turbid solutions (Fig. 9a). Adding polydopamine cross-links the PPMs microspheres, exploiting the abundant functional groups (catechol, hydroxyl group, amino group, etc.) [37], the encapsulation of polydopamine increases the contact area between the spheres, so that the PPMs film can maintain long-lasting morphologic stability in water. The solubility of both PMs and PPMs composite films in water was examined by UV-vis spectroscopy, and the results were consistent with the optical photographs (Fig. 9a-b). The concentration of dissolved substances in the PMs films was increasing during 10 h. In contrast, no dissolved material was detected in the PPMs film even after 30 days of immersion, demonstrating their high stability in aqueous phase.

The actual film operating environment is frequently accompanied by multifactorial and complex conditions that present significant challenges to film stability. Therefore, in addition to immersion in pure water, several complex aqueous environments were simulated, including but not limited to cold (0 °C), hot (90 °C), acidic (pH = 2), alkaline (pH = 13), and ethanol (75 % Alc) aqueous environments. Optical photographs of the PPMs film immersed in the above aqueous solutions at different times are shown in Fig. 9c. Meanwhile, the absorption spectra of the solutions at different times were tested by UV–vis spectrophotometer and shown by contour color plots. As can be seen from the optical photographs and color plots, there is no substance

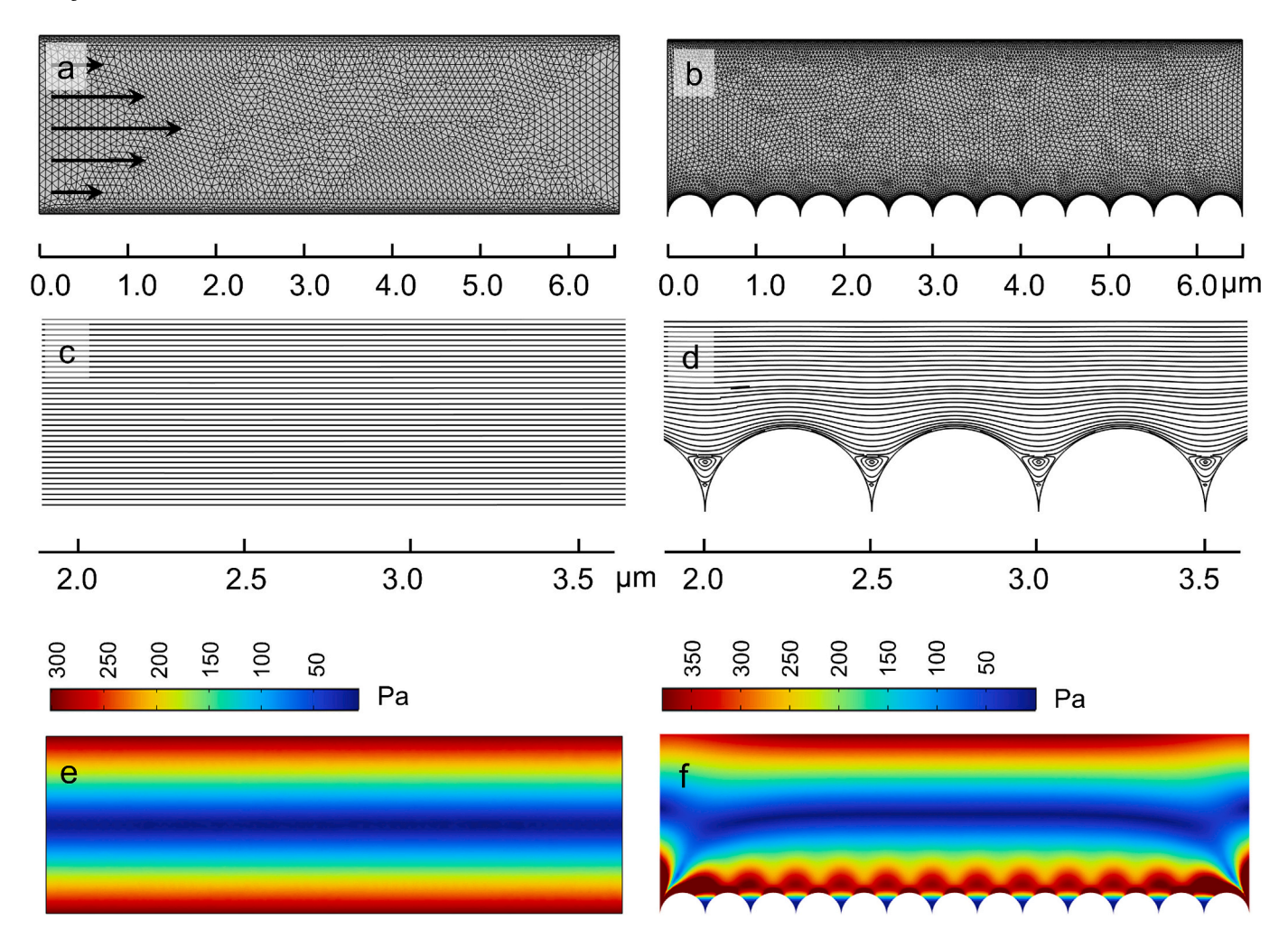


Fig. 8. The geometry and mesh configuration: (a) plane (number of elements: 6556) and (b) spherical (number of elements: 18590). Streamlines in the region of x-coordinate from 2 μm to 3.5 μm, and Contour of shear stress for x-coordinate from 0 μm to 6.5 μm: (c, e) flat film and (d, f) spherical patterned film.

shedding and dissolution phenomenon in cold, hot, acid and ethanol solutions for both films. While the film material has some substances dissolved with time in an alkaline environment, it is presumed that the strong alkaline environment will destroy the bridges between the microspheres [38], resulting in a large number of polypyrrole microspheres dissolved, so the pH of the water environment should be adjusted appropriately in the subsequent separation process.

The changes in the mechanical properties of composite films after immersion in different aqueous environments can reflect the influence of the aqueous environment on their structures. Therefore, we studied the rheology under various conditions, and the resulting stress-strain curves, tensile strengths, and Young's modulus of PPMs films are given in Fig. 9d-e. Due to the low effect of pure water on the connection between fibers and the adhesion between microspheres, the PPMs films had high tensile strength (10.46 MPa), destructive strain (1.81 %), and Young's modulus (775.49 MPa) after immersion in pure water. With the change in the aqueous environment, the mechanical properties of PPMs films were all reduced to different degrees. The tensile strengths were 8.81, 9.15, 9.76, and 7.45 MPa after treatment with cold, hot, acid, and ethanol environments, respectively; the destructive strains were 1.91, 2.25, 1.51, and 1.62 %; and Young's moduli were 661.82, 627.09, 794.60, and 600.52 MPa, respectively. Heat treatment enhances the structural order of intermolecular rearrangements, especially solvation in the non-crystalline regions. In this context, heat treatment reduces the resistance to inter-structural slip, and leads to an increase in the destructive strain (elongation at break). After treatment in an alkaline environment, the tensile strength was 4.94 MPa, and the destructive strain was 0.86 %, which were 2.11 and 2.10 times lower than that of pure water-soaked PPMs film, respectively. In accordance with the results in Fig. 9a, the degradation of polydopamine in alkaline environments causes the detachment of microspheres, which accounts for the decrease in mechanical properties. The deprotonation of polypyrrole by OH breaks the weak hydrogen bonds between the molecular chains, which leads to a decrease in the breaking strain and Young's modulus. These freestanding PPMs films are also robust and flexible, and they can bend or fold multiple times without damage. Meanwhile the PPMs membranes still preserve their separation properties for dyes/salts after 10 bending cycles (Fig. S17). In addition, the PPMs films after immersing in various aqueous environment still preserve their stable dye/salt separation property, only the alkaline treatment leads to slight decrease of separation efficiency of PPMs film (Fig. S18-19). In summary, the prepared PPMs film showed applicability in various complex aqueous environment, offering the possibility of coping with extreme environmental specialty separations.

3. Conclusions

This work reports the development of synthetic mimics of the water purification action of natural sand and gravel structures via the construction of composite films of polydopamine-coated polypyrrole microspheres (PPMs) with graded pore-channel structures using a particle accumulation-space filling method. In addition to the selective dyes/

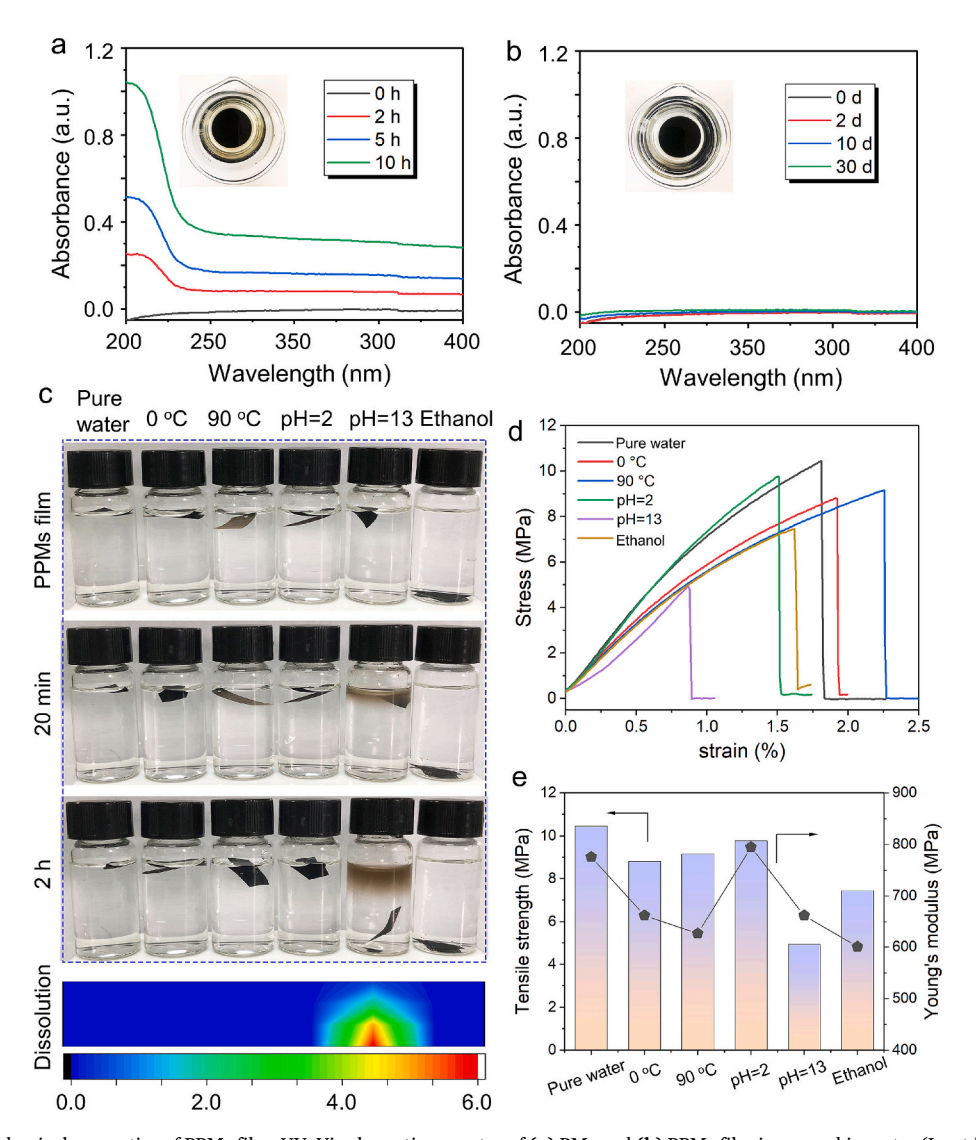


Fig. 9. Stability and mechanical properties of PPMs film. UV–Vis absorption spectra of (a) PMs and (b) PPMs film immersed in water (Inset is optical photographs of PMs and PPMs film after 10 h and 30 d of immersion in water); (c) Morphological stability and substance dissolution rates of PPMs film in different aqueous environments; (d) Stress-strain curves of PPMs film after immersion in different aqueous environments; (e) Tensile strength and Young's modulus of PPMs film after immersion in different aqueous environments.

salts' separation on PPMs surface, we also elaborated the distribution state and behavior of organic dyes by a mathematical fouling model, which demonstrated that the dye only acted on the surface of the film, with less effect on the internal pores. It is this property of the film-solute interface that gives PPMs film excellent contamination resistance. CFD simulations further explain the positive effect of the microstructure of the microsphere arrangement on the removal of contaminants, which opens the way for patterning the surface microstructure in film contamination resistance studies. In addition, the structural characteristics of PPMs film give them long-term stability in different aqueous environments and low environmental burdens, indicating their potential for real, practical applications.

Declaration of competing interest

The authors declare that they have no known competing financial interests or personal relationships that could have appeared to influence the work reported in this paper.

Acknowledgements

The authors would like to acknowledge the financial support from the Fundamental Research Funds for the Jiaxing University (No. 70524006), Jiaxing University Laboratory Open Fund (No. JJ20240031) and Key Laboratory Fund of Jiaxing City (EMN2024-1).

Appendix A. Supplementary data

Supplementary data to this article can be found online at $\frac{https:}{doi.}$ org/10.1016/j.desal.2024.118262.

References

- T. Zhang, H. Tan, Y. Du, et al., Efficient and selective film separation of organism/ salt with graded nanofluid channels stimulated by a rigid crystal skeleton [J], J. Mater. Chem. A 11 (2023) 2367–2376.
- [2] N.K. Hundessa, C.-C. Hu, D.-Y. Kang, et al., Ultra-high flux loose nanofiltration membrane based on metal organic framework (CAU-10-H)/P84 co-polyimide for dye/salt fractionation from industrial waste water [J], Desalination 586 (2024) 117821
- [3] L.-H. Xu, S.-H. Li, H. Mao, et al., Highly flexible and superhydrophobic MOF nanosheet membrane for ultrafast alcohol-water separation [J], Science 378 (2022).

[4] F. Soyekwo, X. Mao, R. Nie, et al., Protein-polyphenol nanoassemblies modulated construction of zeolitic imidazole framework-67 based nanofiltration membrane for effective separation of dye/salt mixtures [J], Desalination 581 (2024) 117532.

- [5] Y. Wang, Y. Zhang, H. Zuo, et al., Enhancing the permeability and selectivity of graphene oxide membrane through polyhedral oligomeric silsesquioxane intercalation for textile wastewater treatment [J], Desalination 587 (2024) 117933.
- [6] M.A. Restrepo, S. Emonds, A. Zhao, et al., Self-supporting biocatalytic polyelectrolyte complex hollow fiber membranes via salt-dilution induced phase separation [J], J. Membr. Sci. 689 (2024) 122157.
- [7] S. Ren, G. Huang, Y. Yao, et al., Integrating radical polymerization and non-solvent induced phase inversion strategy for functionalized ultrafiltration membrane fabrication [J], Desalination 573 (2024) 117220.
- [8] D. You, Z. Feng, J. Wu, et al., Highly permselective and conductive composite anion exchange membranes QPT@PE for electrodialysis desalination [J], Desalination 574 (2024) 117240.
- [9] C. Wei, R. Qiang, L. Lin, et al., Combing three-dimensional water channels and ultra-thin skin layer enable high flux and stability of loose polyimide/SiO₂ nanofiltration membranes at low operating pressure via one step in-situ modification [J], J. Membr. Sci. 623 (2021) 118944.
- [10] J. Li, J.L. Gong, S.Q. Tang, et al., Efficient decolorization performance of graphene quantum dots modulated nanofiltration membranes with tunable pore size for precise molecular sieving [J], Desalination 583 (2024) 117666.
- [11] Y.-Y. Yao, T. Wang, L.-G. Wu, et al., PES mixed-matrix membranes incorporating ZIF-8@MXene nanocomposite for the efficient dye/salt separation [J], Desalination 543 (2022) 116116.
- [12] W.H. Zhang, M.J. Yin, Q. Zhao, et al., Graphene oxide membranes with stable porous structure for ultrafast water transport [J], Nat. Nanotechnol. 16 (2021) 337–343.
- [13] C. Wang, H. Zhang, Y. Wang, et al., A general strategy for the synthesis of hierarchically ordered metal-organic frameworks with tunable macro-, meso-, and micro-pores [J], Small 19 (2023) 2206116.
- [14] Q. Le, Z. Cheng, Template-synthesized nano-Ag₂O@HNTs-constructed hierarchical porous-structured PAN composite nanofiber membrane towards selective adsorption desulfurization [J], Colloids Surf. A Physicochem. Eng. Asp. 655 (2022) 130242.
- [15] P.M. Gurave, S. Dubey, B. Nandan, et al., Pickering emulsion-templated nanocomposite membranes for excellent demulsification and oil-water separation [J], ACS Appl. Mater. Interfaces 14 (2022) 54233–54244.
- [16] F. Li, J. Meng, J. Ye, et al., Surface modification of PES ultrafiltration membrane by polydopamine coating and poly(ethylene glycol) grafting: morphology, stability, and anti-fouling [J], Desalination 344 (2014) 422–430.
- [17] Q. Liu, P. Huang, N. Xu, et al., Decoupling synthesis and crystallization of covalent organic frameworks (COFs) for more crystalline layer targeting high efficiency dye separation [J], Sep. Purif. Technol. 341 (2024) 126881.
- [18] L. Riley, P. Cheng, T. Segura, Identification and analysis of 3D pores in packed particulate materials [J], Nat. Comput. Sci. 3 (2023) 975–992.
- [19] X. Ding, Y. Fan, N. Xu, A new route for the fabrication of TiO₂ ultrafiltration membranes with suspension derived from a wet chemical synthesis [J], J. Membr. Sci. 270 (2006) 179–186.

- [20] Q. Wang, W. Lin, S. Chou, et al., Patterned membranes for improving hydrodynamic properties and mitigating membrane fouling in water treatment: a review [J], Water Res. 236 (2023) 119943.
- [21] Y. Guan, W. Zhang, B. Bi, et al., Polypyrrole-mediated construction of superhydrophobic photo/electro thermal composite fabric for efficient crude oil dehydration and recovery [J], Desalination 591 (2024) 117978.
- [22] U. Baig, A. Waheed, A facile strategy for fabrication of nanocomposite ultrafiltration membrane: oily wastewater treatment and photocatalytic selfcleaning [J], npj Clean Water 6 (2023) 68.
- [23] J. Yu, T. Marchesi D'alvise, I. Harley, et al., Ion and molecular sieving with ultrathin polydopamine nanomembranes [J], Adv. Mater. 36 (2024) 2401137.
- [24] Y. Li, J. Yan, H. Liu, et al., Preparation of MOFs-based molecularity imprinted composite membrane biomimetically modified by PDA and its selective separation performance and mechanism [J], Desalination 581 (2024) 117622.
- [25] T. Zhang, R. Guo, G. Ying, et al., Absolute film separation of dyes/salts and emulsions with a superhigh water permeance through graded nanofluidic channels [J], Mater. Horiz. 9 (2022) 1536–1542.
- [26] S. Ling, K. Jin, D.L. Kaplan, et al., Ultrathin free-standing bombyx mori silk nanofibril membranes [J], Nano Lett. 16 (2016) 3795–3800.
- [27] F. Yang, F. Tao, C. Li, et al., Self-assembled membrane composed of amyloid-like proteins for efficient size-selective molecular separation and dialysis [J], Nat. Commun. 9 (2018) 5443.
- [28] M.J. Corbaton Baguena, S. Alvarez Blanco, M.C. Vincent Vela, Fouling mechanisms of ultrafiltration membranes fouled with whey model solutions [J], Desalination 360 (2015) 87–96.
- [29] I.M. Griffiths, A. Kumar, P.S. Stewart, A combined network model for membrane fouling [J], J. Colloid Interface Sci. 432 (2014) 10–18.
- [30] F. Bai, S. Liu, Y. Zhang, et al., Effective and mechanistic insights into reverse osmosis concentrate of landfill leachate treatment using coagulation-catalytic ozonation-bioaugmentation-based AnMBR [J], Chem. Eng. J. 463 (2023) 142430.
- [31] L. Yang, X. Zhang, J. Rahmatinejad, et al., Triethanolamine-based zwitterionic polyester thin-film composite nanofiltration membranes with excellent foulingresistance for efficient dye and antibiotic separation [J], J. Membr. Sci. 670 (2023) 121355.
- [32] A.R. Kuzmyn, L.W. Teunissen, P. Fritz, et al., Diblock and random antifouling bioactive polymer brushes on gold surfaces by visible-light-induced polymerization (SI-PET-RAFT) in water [J], Adv. Mater. Interfaces 9 (2022) 2101784.
- [33] A.R. Kuzmyn, A.T. Nguyen, L.W. Teunissen, et al., Antifouling polymer brushes via oxygen-tolerant surface-initiated PET-RAFT [J], Langmuir 36 (2020) 4439–4446.
- [34] Y. Liu, J. Ran, Q. Guo, et al., Advancements in nanofiltration fouling phenomenon: from water treatment to salt lakes environments [J], Desalination 583 (2024) 117649.
- [35] Y.K. Lee, Y.-J. Won, J.H. Yoo, et al., Flow analysis and fouling on the patterned membrane surface [J], J. Membr. Sci. 427 (2013) 320–325.
- [36] J. Chen, S. Xu, C.Y. Tang, et al., Stability of layer-by-layer nanofiltration membranes in highly saline streams [J], Desalination 555 (2023) 116520.
- [37] E. Kozma, A.E. Andicsova, A.O. Siskova, et al., Biomimetic design of functional plasmonic surfaces based on polydopamine [J], Appl. Surf. Sci. 591 (2022) 153135.
- [38] J. Yang, A. Xie, J. Cui, et al., An acid-alkali-salt resistant cellulose membrane by rapidly depositing polydopamine and assembling BaSO₄ nanosheets for oil/water separation [J], Cellulose 27 (2020) 5169–5178.